AMPDXA for Precision Bone Loss Measurements on Earth and in Space

Harry K. Charles Jr., Michelle H. Chen, Thomas S. Spisz, Thomas J. Beck, Howard S. Feldmesser, Thomas C. Magee, and Barry P. Huang

Bone loss and its strength-related implications are major health concerns for our aging earthbound population and for astronauts exposed to microgravity during long-duration spaceflight. Key to understanding the causal mechanisms of both age-related osteoporosis and microgravity-induced bone loss is the ability to make precision bone loss and bone structural measurements. The Advanced Multiple-Projection Dual-energy X-ray Absorptiometry (AMPDXA) scanning system is being developed at APL to meet this need. This article describes the development of the AMPDXA system, funded by the National Space Biomedical Research Institute (NSBRI), over the last several years, including progress made in human bone imaging, bone mineral density determination, and bone structural measurements. It also presents general information on bone loss, the efficacy of bone loss countermeasures, and the inherent differences between age-related osteoporosis and microgravity-induced bone loss. The current effort will continue for the next 4 years and will culminate in the delivery to the NSBRI and NASA of a ground-based clinical system suitable for pre- and postflight testing of astronauts.

BACKGROUND

The continued manned exploration of space is fraught with many technological, financial, and political issues as well as significant and potentially life-threatening health problems caused by the effects of radiation and microgravity (weightlessness) on the human body. A serious health issue is microgravity-induced muscle wasting and bone loss encountered by astronauts in long-duration space missions.[1] Already, scientists have observed significant bone loss, characterized by a reduction in bone mineral density (BMD), in astronauts during space missions of up to 6 months in duration. This microgravity-induced loss in BMD has occurred primarily in the weight-bearing portions of the human skeletal system (i.e., spine, pelvis, and femur). In these critical weight-bearing bones, astronauts can lose between 1 and 2% of their BMD per month and suffer structural and functional changes in bones, muscles, and connective tissues.[2,3] Cosmonaut bone loss in regions of the femur for missions of up to 180 days is shown in Fig. 1. In comparison, a postmenopausal woman on

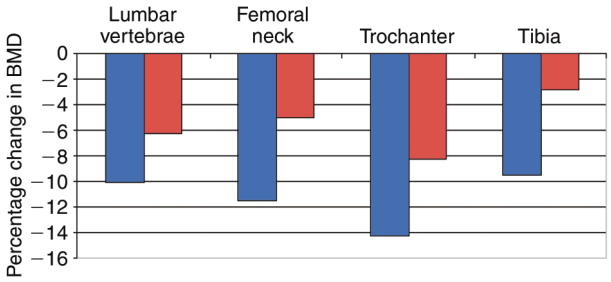

Figure 1. Percentage change in bone mineral density (BMD) of femur regions for cosmonauts on space missions of up to 180 days (blue and red are maximum and average gain/loss in BMD, respectively).

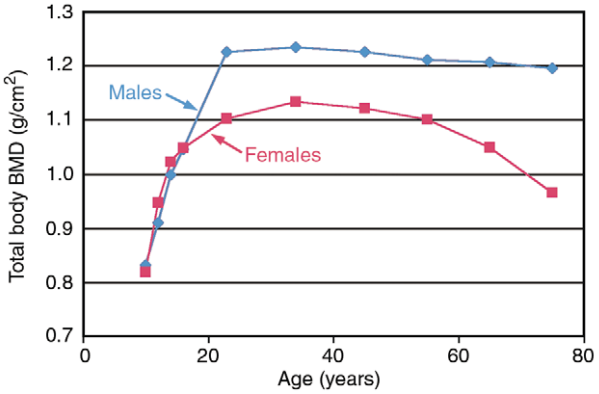

Figure 2. Bone density with age profiles.

Earth will lose about 1% of her BMD per year.[4] After a year of spaceflight, astronauts could be expected to lose about 20% of their BMD, which would correspond to an approximate 40% loss in bone strength. Such losses in strength would cause serious problems when the astronaut returns to Earth. Even setting foot on Mars, where the gravity levels are 3/8 of the Earth's gravity, would present a high risk of fracture. A fracture on a remote planetary surface would be at best serious and at worst fatal because of the lack of extensive medical facilities and inhibition of fracture healing[5] caused by microgravity or reduced gravitational fields. Also, it would mean an increased workload on the remaining crew members.

Bone Loss

Osteoporosis

Bone loss is not just a concern of those who spend prolonged periods of time in microgravity; in fact, every man, woman, and child on Earth needs to be concerned with bone loss. On Earth, the average person will experience increasing BMD until approximately 35 years of age and thereafter will begin to lose BMD steadily. This loss of bone is most prevalent in women, especially after menopause. Figure 2 illustrates typical bone density with age profiles for both men and women.

Forty percent of postmenopausal women can be expected to develop osteoporosis, a disease characterized by extremely low BMD. Osteoporosis is a worldwide problem and, as the global population ages, more and more people will be afflicted with osteoporosis and osteopenia (a condition of below-average bone density). In the United States alone, an estimated 10 million people, 80% of whom are women, suffer from osteoporosis. Another 34 million suffer from osteopenia. Those with osteopenia have about a 50% risk of developing osteoporosis and the further risk of suffering a fracture. It is estimated that osteoporosis is responsible for more than 1.5 million fractures per year, with an annual estimated cost of over $20 billion (2003 estimate) in health care.[6] To put these numbers in perspective, osteoporotic-related fractures exceed diagnosed breast cancer cases (180,000 per annum) by a factor of 8. Hip fractures in Americans aged 45 and older number 300,000 annually. In addition to the sheer numbers and the associated health care costs, osteoporosis claims a steep human price. Twenty-four percent of those aged 50 or older who suffer a hip fracture die within a year, usually as a result of complications from extended bed rest, such as a pulmonary embolus, where a blood clot in the thigh or pelvic region breaks off and travels to the lungs. The clot can then block a major blood vessel, causing death if not treated quickly. Of those who do recover from hip fracture, approximately 50% will never walk unassisted again. By 2020, it is estimated that nearly 1800 hip fractures will occur daily. As the baby boom generation ages, the costs and numbers of people with osteoporosis will increase significantly.

Earth Loss Mechanisms

The basic structural unit of bone is a hollow rod of collagen and calcium phosphate. In the shaft of the bone, these rods are bundled in parallel and arranged in a ring of compact bone, forming a hard cortical shell. This shell provides maximum resistance against compressive and bending forces and protects the marrow within. Toward the end of the bone, where stresses become more complex, the rods of the cortical shell splay out to form a complex network of trabecular bone, also known as cancellous or spongy bone. The greatest loss of BMD occurs in the trabecular bone. Bones containing high amounts of trabecular bone include the hip, the femur, and the heel, which are all located in high load-bearing regions and thus are subject to complex stresses.

Human bones continually undergo processes of growth and resorption. Cells called osteoblasts lay down new bone in a process called mineralization. Other cells called osteoclasts absorb and remove old bone in a process known as resorption. As a normal child grows, the

rate of mineralization is much greater than the rate of resorption. The mineralization and resorption rates generally stabilize and remain relatively unchanged until the early- to mid-30s, when the resorption rate begins to exceed the rate of mineralization. This increase in resorption rate is especially pronounced in postmenopausal women.

Despite net bone loss as a person ages, new bone is still added slowly to the outside of the cortical shell, while old bone is resorbed from the inner cortical shell and the trabecular region. The result is a larger-diameter or wider bone, as evidenced by bony knuckles in the elderly, with a much thinner cortical shell and a more widely spaced trabecular network. These changes cause the bone to be more fragile, yet allow it to preserve much of its strength.[7] In osteoporotic patients, the rate of bone resorption is significantly accelerated, which leads to thinning of bone cortices and trabecular elements. As the trabeculae are thinned and perforated, there is a preferential loss of the horizontal trabeculae; thus, the bone is more susceptible to buckling forces and, hence, a greater propensity for fracture with less force or trauma.

Space Loss Mechanisms

Because of the unloading of mechanical stresses and weight, astronauts in space experience a similar but much faster rate of resorption. The skeleton no longer has to bear the astronaut's full weight and so begins to rid itself of what it believes is unnecessary bone by signaling the osteoclasts to resorb bone at a much faster rate. Microgravity also directly affects the rate of bone formation by slowing or destroying the action of the osteoblasts and reducing the amount of calcium absorption. On Earth, the body absorbs 40 to 50% of the calcium intake, whereas only 20 to 25% is absorbed in space. Astronauts also experience reduced levels of vitamin D, which plays a key role in calcium metabolism. Human skin usually synthesizes vitamin D from the ultraviolet radiation in sunlight. Natural sunlight in spacecraft is limited, causing vitamin D levels in the body to fall and increasing calcium resorption from the skeleton into the blood and urine. These increased levels of calcium resorption also lead to an increased risk of renal stone formation.[8]

NASA, in its Bioastronautics Critical Path Roadmap[9] for space-related health issues, officially calls the space bone loss phenomenon "microgravity-induced acceleration of age-related osteoporosis." However, based on limited studies on bone loss in astronauts compared with an ever-expanding database on earthbound osteoporosis, it has been shown that the mechanisms of microgravity-induced bone loss and age-related osteoporosis differ. In contrast to the accelerated rate of bone resorption (i.e., exceeding the rate of bone growth or mineralization), which is characteristic of osteoporosis, the hypothesized mechanism in space is that osteoblastic activity is significantly inhibited; hence, bone growth or mineralization is greatly reduced or nonexistent. The osteoclasts, however, continue to resorb bone at or above the normal rate, causing the bone as a whole to be thinner (thinner cortical shell) and also weaker, since no compensating bone growth (increase in diameter) occurs to preserve overall bone strength. While osteoporotic bones may be thinner and more fragile than ordinary bones, they can still technically withstand normal loading because of the increase in diameter. Thus, for a given amount of bone loss on Earth and in space, the impact of the loss in space is much more severe and, of course, occurs much more rapidly.

Countermeasures

Although bone loss mechanisms appear to differ on Earth and in space, similar treatments and therapies may be applicable in both situations. The known treatments for osteoporosis fall into three main categories: anti-resorptive measures, bone-building regimens, and non-pharmacological intervention. Most current drug therapies are anti-resorptive, with the specific aim of slowing the rate of bone loss. Bone-building treatments, which are just becoming available, focus on increasing the rate of mineralization. Finally, non-pharmacological intervention, such as exercise, potentially helps reduce the risk of fracture. Most treatments for osteoporosis and bone loss on Earth are based on drug therapy. In space, exercise is the main countermeasure to bone loss, since many anti-resorptive drugs have not yet been approved for spaceflight or have been unsuccessful in their limited application.

Drug Therapy

Several forms of anti-resorptive drug treatments are available for osteoporosis, including hormone replacement therapy (HRT), selective estrogen receptor modulators (SERMs), and nonhormonal drugs (e.g., bisphosphonates and calcitonin). HRT replaces estrogen for peri- and postmenopausal women. It can be administered by means of tablets, skin patches, or creams. HRT not only lessens the effects of menopause but also greatly reduces the rate of postmenopausal bone loss; however, prolonged use of HRT can elevate the risks of breast and uterine cancers. SERMs mimic estrogen only in certain organs and tissues where the effect of estrogen is beneficial and block estrogen receptors in areas where the effect may be harmful. Thus, SERMs can be used to treat menopause-related conditions such as osteoporosis and heart disease without unwanted side effects. Currently, raloxifene, the only available SERM, has been shown to reduce the risk of vertebrate factures by 30 to 50%. Raloxifene is marketed as Evista.

Bisphosphonates inhibit the resorption of bone by the osteoclasts. Nonhormonal bisphosphonates are

readily available in a variety of forms, providing a wide range of therapeutic options. The most extensively studied bisphosphonate is alendronate, which is marketed in tablet form as Fosamax. Alendronate has been shown to increase BMD and decrease fracture risk in both the hip and spine by 50%. Calcitonin, a hormone produced by the thyroid gland, has been shown to inhibit resorption by the osteoclasts. It is available both as a nasal spray and an injection and has been shown to reduce the risk of vertebrate fracture by 25 to 35%. Calcitonin is also known for its pain-relieving effect. To date, no significant health risks have been associated with bisphosphonates or calcitonin.[6]

For more than 70 years, parathyroid hormone (PTH) has been known to have bone-building effects, but only recently have studies confirmed its efficacy. In a multinational study of women with previous vertebral fractures, PTH was found to decrease the risk of another vertebral fracture by as much as 70% and to decrease the risk of nonvertebral fractures by 50%. This improvement occurred within an 18-month window after treatment. While most of the drugs mentioned above have been approved by the FDA for women only, alendronate and a risedronate, another bisphosphonate, are approved for osteoporotic men. Calcitonin has been shown to be equally effective for men but has not received FDA approval for their treatment.

Exercise (and Nutrition)

Appropriate exercise, coupled with sufficient calcium, vitamin D, and protein intake, has been shown on Earth to maintain and even build up bone mass. Taking daily calcium (0.1–1.0 g/day) and vitamin D (800 IU/day) has been proven to reduce the risk of fracture. Although a steady calcium intake throughout life is important, calcium becomes especially significant in late menopause and thereafter. Bone loss in early menopause is caused primarily by estrogen loss, on which calcium has little effect. Postmenopausal bone loss is due to the body's inability to maintain calcium in the blood, so the body draws calcium from the skeletal system. Vitamin D, as noted previously, is an important factor in the regulation of blood calcium. Decreased vitamin D levels lead to increased bone resorption. Adequate protein consumption is also important for maintaining bone mass and muscle function. Regular weight-bearing exercise—running, jogging, walking, etc.—is essential in maintaining bone homeostasis.

Astronauts use several methods of exercise in space to counter bone loss and muscle atrophy.[10] Treadmills and bicycle ergometers have been in use since Skylab and later on Mir. Space treadmills resemble ordinary treadmills on Earth except for an elastic harness used to pull the runner toward the treadmill surface, simulating the loading effects of gravity. Although such loading is necessary to prevent bone loss and muscle atrophy, the tethering system is so uncomfortable that astronauts take breaks every 5 to 10 min, thus preventing adequate cardiovascular conditioning.

Bicycle ergometers are the preferred instrument for cardiovascular conditioning. Early ergometers resembled stationary exercise bikes used on Earth. Newer ergometers have the astronauts lying on their backs with their feet elevated relative to their head. A shoulder brace holds the astronauts in place as they pedal against a resistance load provided by a flywheel and braking system. The ergometer does not try to simulate the loading of gravity; rather, it provides muscle conditioning for the legs.

Both the treadmills and ergometers cause considerable vibration in the spacecraft. Such vibrations can interfere with sensitive onboard experiments and can potentially influence the flight and/or stability of the spacecraft itself. Thus, exercise equipment must be appropriately isolated from the spacecraft with special devices to counteract the vibrations. A relatively new form of exercise involves pulling against bungee cords of various strengths. This minimizes vibrations to the spacecraft and potentially can have as much beneficial effect on bone loss and muscle atrophy as the treadmill/ergometer systems.

All of these systems, however, are relatively ineffective against bone loss and muscle atrophy.[10] One reason is that even though the effects of skeletal loading on bone growth have been studied for nearly 40 years, minimum loading thresholds necessary to achieve osteogenic effects are still unknown. A new dynamic exercise device has been developed[11] in which a jumping-type exercise has produced peak external forces from 1.7 to 4.0 times the body weight. It is believed that such loads are sufficient to stimulate bone growth. Because the generation of these significant forces can produce loads on the spacecraft, special isolation and vibration damping methods are being developed.

As mentioned above, drugs, exercise, and other forms of intervention have met with limited success in preventing bone loss and muscle atrophy in space. Of the drugs, alendronate has shown the most potential and appears to be effective in both men and women. Drugs in combination with exercise may offer some hope. Common sense seems to dictate that resistive exercises such as weightlifting or rowing will help offset bone loss. Yet, consistent bone loss was experienced by both American astronauts and Russian cosmonauts on Mir despite regular exercise (up to 4 h per day), indicating that additional bone loss mechanisms in space are involved.

Perhaps the only way to prevent bone loss in space will be to introduce artificial gravity. Artificial gravity research has begun anew, with scientists looking at personal centrifuges that create 1-*g* forces at an astronaut's feet rather than the huge rotating space station concept of the 1950s with diameters greater than 1 mile. The

personal centrifuges would be used for a period of time each day, much like today's exercise machines.

The ultimate answer to preventing bone loss in space may lie in the methods described or in something that has not yet been developed. Either way, the key to a successful solution will be the ability to make precision bone loss measurements—first on Earth and then in flight. The development of such an instrument at APL—the Advanced Multiple-Projection Dual-energy X-ray Absorptiometry (AMPDXA) sensor system—is the focus of the remainer of this article. This effort has been funded by the National Space Biomedical Research Institute (NSBRI),[12] a consortium of 12 leading medical and research institutions funded by NASA.

BONE LOSS MEASUREMENTS

Recall that osteoporosis is a disease in which the rate of bone resorption greatly exceeds the rate of bone formation. A patient is officially considered to have osteoporosis if he or she has a T-score of –2.5 or less, i.e., the person's BMD is 2.5 or more standard deviations below the average BMD for a young adult (25–30 years old) of the same gender. The current standard for making BMD measurements and determining T-scores is dual-energy X-ray absorptiometry (DXA or DEXA).[13] Sometimes the DXA results are given in terms of a Z-score. The Z-score is the number of standard deviations from the age-matched average BMD for healthy individuals and, therefore, takes into account the average bone loss expected as a result of aging (Fig. 2).

In DXA, two low-dose X-ray beams of different energies are used to scan regions of the body that are vulnerable to or suspected of bone loss. Since two different X-ray energies are used, areas of soft tissue and bone can be separated. Bone and muscle (soft tissue) absorb differently at the different source energies. Thus, for each point scanned, two attenuation values are produced—one for high energy and one for low energy. These attenuation data are then converted into bone and muscle equivalents by comparing the results to attenuation measurements performed on a calibration phantom composed of varying thicknesses and combinations of aluminum (simulates bone absorption) and plastic (simulates soft tissue or muscle absorption). Subtraction of either the bone or muscle attenuation from the total attenuation indicates muscle or bone, respectively, at that scan point. Combining all the scan points produces a two-dimensional (2D) image or projection of the muscle or bone. The final measurements derived from the DXA scan are compiled into a BMD report.

BMD is not a density in the traditional sense of mass per unit volume (e.g., g/cm^3), but rather a 2D projected density of the mineral mass in the bone measured in g/cm^2. The 2D image of the bone is divided into regions, and the BMD is calculated by dividing the average bone mineral content of the region (as calculated from the X-ray attenuation mapping) by the area of the region. Conventional BMD measurements, however, are limited. By collapsing the bone into a 2D representation, important information about the 3D density, geometry, and structural strength is lost. The BMD results do not distinguish between compact and cancellous bone; hence, all bone is lumped into a single total density measurement. Subsequently, it is difficult (or impossible) to reconstruct an engineering model of the bone to perform stress loading and fracture simulations.

Full-body DXA is the current measurement method of choice for assessing BMD and total body composition because it uses a very low radiation dose, is accurate with a high degree of precision, makes measurements rapidly, is convenient and easy to use, and is relatively inexpensive. Several other methods for measuring BMD, bone structure, and soft tissue include magnetic resonance imaging,[14] ultrasound,[15–17] and computed tomography. Although these techniques have advantages over DXA under certain limited circumstances, only DXA has been certified by the FDA for diagnosing and monitoring osteoporosis. The effective dose equivalent of a conventional DXA scan is less than 10^{-5} Sv, which is less than half the radiation dose of a chest X-ray. This is roughly equivalent to the natural background radiation dose experienced by a person on Earth during a day at the seashore. The International Commission on Radiological Protection recommends an annual dose of no more than 1 Sv per year for the general public. Consequently, repeated DXA scans used in longitudinal studies can be made at closely spaced intervals in time without adverse effects.

THE AMPDXA PROJECT

Design

Given the limitations of other techniques and the need to determine both the specific location of bone loss and geometrical changes in bone structure to fully assess the risk of fracture to astronauts in space and to those suffering osteoporosis on Earth, a proposal for a flight-qualifiable AMPDXA system to measure bone loss and structure was made to the NSBRI in 1997 by a joint team from APL and the Johns Hopkins School of Medicine. The project was funded for calendar year 1998 and has had a series of renewals over the last 6 years, including the latest 4-year project which started in September 2004. The focus of this latest project is the development of the Ground-based Clinical System (GCS) for use in pre- and postflight astronaut testing at Johnson Space Flight Center in Houston, Texas.

Initially, the project concentrated on developing multiple projection principles and algorithms for the extraction of high-resolution BMD images containing structural information while also developing two

ground-based test systems: a laboratory test bed (LTB; Fig. 3) and a human test bed (HTB; Fig. 4).[18] As these ground-based instruments were being developed, system concept studies for a flight prototype were being performed. The goal of these studies was to conceptually design an AMPDXA suitable for spaceflight. This required a strong lightweight structure, compact electronics, and tight power budgets to allow its use on the Space Station or on a manned planetary expedition. We believe that an ultimate weight of 46 kg (100 lb) is possible.

As mentioned above, the AMPDXA scanner system has been designed to measure BMD and bone geometry (cross sections, section moduli, etc.). By using multiple images acquired at different angles, it is possible to extract highly precise BMD and bone geometry images that allow the creation of accurate bone structural models which can be used for fracture assessment. In addition, the AMPDXA allows the extraction of cross-sectional areas of muscle, muscle volume, and volumetric densities of lean and fat tissues. A synergistic by-product is that the multiple projections minimize or eliminate the measurement errors associated with patient positioning. Consequently, the AMPDXA could be used for longitudinal studies of bone and muscle in space. The AMPDXA scanner system has been expressly designed to overcome the limitations that govern DXA's poor performance, including image resolution, image noise, the effects of two dimensions, and specific measurement site location.

Figure 3. Laboratory test bed for the development and proof of AMPDXA principles of operation.

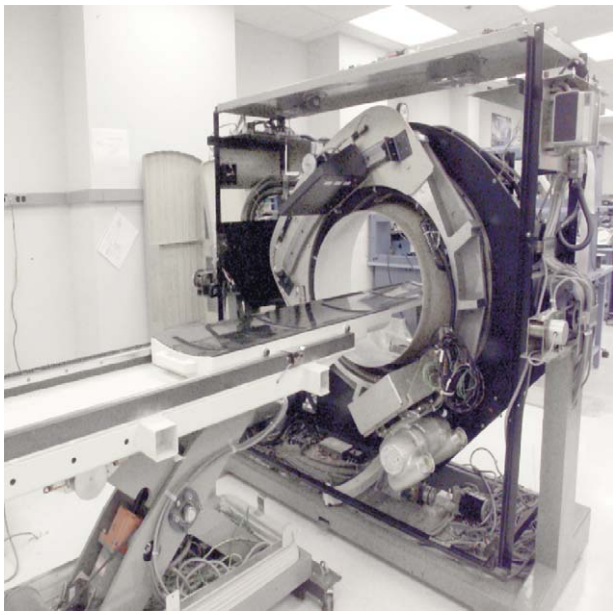

Figure 4. The AMPDXA human test bed in a clinical setting with covers removed.

Image Resolution

Conventional DXA scanners produce relatively coarse images with pixel spacing on the order of 1 mm or larger, so objects smaller than about 2–3 mm typically cannot be resolved. This poor resolution limits the ability to reliably measure bone dimensions, especially since small differences are mechanically significant. Our analyses suggest that resolution needs to be on the order of 0.5 mm or less for small children. The AMPDXA HTB has pixel spacing of about 0.25 mm and spatial resolution in the patient plane of about 0.3 mm, thus meeting the design goals. The ground-based clinical system to be built in the next phase will have a comparable resolution. By varying the table height, it may be possible to increase the resolution for scanning small children and decrease the resolution for osteoporosis screening.

Image Noise

When bones are very thin, as in the case of osteoporosis or very small bones, image noise limits the ability to distinguish bone from surrounding soft tissues. Noise in DXA depends on two factors: (1) the amount of X-rays that travel through the patient to the detectors and (2) the separation between the two X-ray beam energies. Most DXA scanners operate with the same amount of X-rays independent of patient size, so image noise gets worse with "thicker" patients. The AMPDXA HTB successfully tested a method for adjusting the X-ray flux so that it is optimal for patients of different thicknesses. The HTB also tested an X-ray beam configuration that was more optimal in energy separation than conventional DXA scanners.

Two-Dimensional Limitations

A conventional DXA image is a 2D projection of a 3D bone. Lines of pixels across the bone axis in the image are projections of the corresponding cross sections from which the geometry can be derived for bending in the image plane. If the bone cross section is symmetric about its long axis, the geometry derived in this way describes bending strength in any direction. However,

most bones are not axially symmetric and are stronger in some bending directions than in others, and the single projection only measures one direction. If the bone is rotated between sequential measurements, it is impossible to determine if the strength actually has changed or if the change is the result of a change in rotation of an asymmetric bone.

The AMPDXA was specifically designed to solve this problem by providing images from a small number of projections from which the geometry for bending in any direction can be obtained. In engineering terms, the principal (maximum and minimum) moments of inertia are derived (see the boxed insert). The original idea was to generate projections at 0°, 45°, and 90° about the bone axis. It was later realized that, with some additional mathematics, the moments of inertia could be derived from three projections over a smaller angular range as shown below. This was implemented in hardware using projections at 0° and ±15° in either direction from the central projection. Results were demonstrated on the HTB version of the AMPDXA.

Measurement Site Location

Bone location is the most important source of imprecision in patient measurement. Cross-sectional dimensions must be measured at cut planes that traverse the long axis of the bone at known locations. These cut planes must lie in the same relative position in all

PRINCIPAL MOMENTS OF INERTIA

The method for determining the principal moments of inertia uses three projections, two of which are symmetrically located about the centrally located third projection. First, it is an engineering principle that any two orthogonal, cross-sectional moments of inertia (I_x, I_y) sum to a constant (the polar moment of inertia I_p) that is equivalent to the sum of the principal moments of inertia (I_{max}, I_{min}):

$$I_p = I_x + I_y = I_{max} + I_{min} . \quad (1)$$

The two cross-sectional moments of inertia can be obtained from any two orthogonal AMPDXA projections of the bone. The principal moments of inertia are given by

$$I_{max} = \frac{I_x + I_y}{2} + \sqrt{\left(\frac{I_x - I_y}{2}\right)^2 + I_{xy}^2} \quad (2)$$

and

$$I_{min} = \frac{I_x + I_y}{2} - \sqrt{\left(\frac{I_x - I_y}{2}\right)^2 + I_{xy}^2} , \quad (3)$$

where I_{xy} is the product of inertia. The product of inertia can be obtained by using the rotation of axes for moments of inertia. The moment of inertia I_θ at some angle θ from the x axis is

$$I_\theta = \frac{I_x + I_y}{2} + \frac{I_x - I_y}{2}\cos(2\theta) - I_{xy}\sin(2\theta) . \quad (4)$$

Solving for I_{xy} yields

$$I_{xy} = \frac{\frac{I_x + I_y}{2} + \frac{I_x - I_y}{2}\cos(2\theta) - I_\theta}{\sin(2\theta)} . \quad (5)$$

The above methodology can be used with an AMPDXA scanner capable of rotating about the long axis of a bone by at least 90°. A common problem is that it is difficult to obtain projections over a 90° range because of the overlap of other bones or the orientation of the bone axis, such as that encountered in the femoral neck where osteoporotic failures commonly occur. To solve this problem, the AMPDXA-GCS will use three projections over a smaller rotational angle, e.g., 30° (±15° about a zero reference) to obtain the moments of inertia (I_x, I_θ, and I_{θ_2}), provided $\theta_1 = -\theta_2$. The orthogonal moment of inertia I_y can then be derived as follows.

Beginning with the rotated axis formula, as given in Eq. 4, the moment of inertia I_{θ_1} at angle θ_1 is calculated:

$$I_{\theta_1} = \frac{I_x + I_y}{2} + \frac{I_x - I_y}{2}\cos(2\theta_1) - I_{xy}\sin(2\theta_1) . \quad (6)$$

Similarly, I_{θ_2} is calculated for the projection at angle θ_2:

$$I_{\theta_2} = \frac{I_x + I_y}{2} + \frac{I_x - I_y}{2}\cos(2\theta_2) - I_{xy}\sin(2\theta_2) . \quad (7)$$

Summing I_{θ_1} and I_{θ_2},

$$I_{\theta_1} + I_{\theta_2} = I_x + I_y + \frac{I_x - I_y}{2}[\cos(2\theta_1) + \cos(2\theta_2)] - I_{xy}[\sin(2\theta_1) + \sin(2\theta_2)] . \quad (8)$$

Since $\cos(2\theta_1) = \cos(2\theta_2)$ and $\sin(2\theta_1) = -\sin(2\theta_2)$, Eq. 8 reduces to

$$I_{\theta_1} + I_{\theta_2} = I_x + I_y + \frac{I_x - I_y}{2}[2\cos(2\theta_1)] . \quad (9)$$

And then solving for I_y,

$$I_y = \frac{I_{\theta_1} + I_{\theta_2} - I_x[1 + \cos(2\theta_1)]}{1 - \cos(2\theta_1)} . \quad (10)$$

Then I_x is associated with the center direction, and I_y is calculated using Eq. 10. The principal moments of inertia are subsequently found by using Eqs. 2 and 3 in conjunction with Eq. 5.

individuals, regardless of size and shape. When DXA scans are repeated, often years apart, the same locations on the bone must be measured. The problem is exacerbated since one cannot reliably identify cut plane locations on bones embedded within the body by using superficial landmarks, i.e., points on the skin that can be felt or seen. The most common solution to this problem is to image the entire volume of the patient containing the bone of interest, then retrospectively orient the cut planes using image analysis methods. To fully reconstruct the cut plane with the required precision, the screening mechanism must be able to image the entire volume with the same resolution in all directions. In the commercial world, only the latest-generation multislice X-ray computed tomography scanners can make measurements with equal resolution along all three axes.

While high-resolution volume imaging is possible with these devices, the radiation dose is much higher than with a DXA scanner, so high, in fact, that it would be prohibitive for use in screening subjects for weak bones, repeated use in treatment follow-up, and use in small children. Using the AMPDXA prototypes, we investigated a range of solutions and finally produced the design that is to be built in the next phase. This design solves the problem by rapidly scanning the entire bone in two projections. The two-projection data are then used to locate the bone axes in 3D space, where cut planes are to be placed. The scanner then moves to specific sites and orients the scanning mechanism so that projections are aligned in planes orthogonal to the local bone axis. The scanner rapidly generates 32 cut planes in three projections in a single pass over the patient. It then moves to the second region, re-orients itself, repeats the three-projection scan, and so on. A particular bone will probably be defined by three to five sets of these scanning traverses.

Project Execution

Currently, the AMPDXA project is focused in three primary areas: (1) instrument development, (2) algorithm development for BMD image extraction and structural analysis, and (3) bone reconstruction and modeling techniques. The instruments developed include a full-sized (1-m source-to-detector distance) LTB and an HTB. The LTB (Fig. 3) was used to verify principles and theoretical predictions and to demonstrate that the AMPDXA techniques worked and produced results with expected precision. Such results are shown in Fig. 5. Figure 5a is an AMPDXA BMD image of a human femur immersed in a cylinder of water (simulates fatty tissue). The same bone was imaged on a new, commercial DXA scanner at Johns Hopkins Hospital (Fig. 5b). The improvement in spatial and contrast resolution is quite evident in the figure.

The HTB (Fig. 4) incorporates high-precision rotational and translational stages to provide the scanning capability to perform qualification tests on human subjects. Since the HTB is designed to operate only on Earth, the table, gantry, and associated equipment were not built to the size and mass requirements of an AMPDXA unit for spaceflight. In fact, it was built from a used computer tomography scanner. Buying used equipment for some of the structured elements and rotating parts and machinery allowed critical project resources to be focused on information extraction and analysis issues leading to human testing.

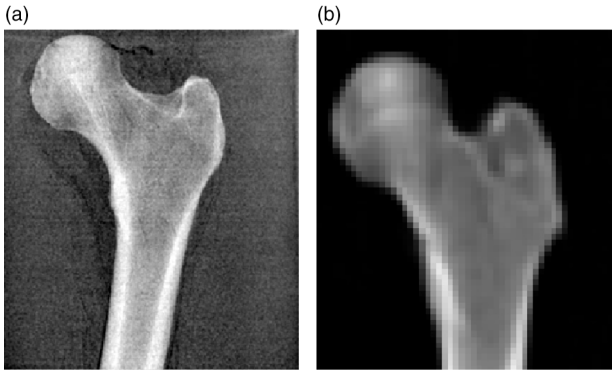

Figure 5. Comparison of (a) an AMPDXA BMD image and (b) a BMD image taken with a conventional DXA (same human cadaver bone).

Fine-structure detail in the BMD spatial projections (Fig. 6) is reproducible and provides information on the bone's microstructure. The AMPDXA enables cross sections to be determined at any point along the bone, thus allowing accurate reconstruction of the bone geometry for structural modeling and the ultimate determination of a fracture risk. Figure 7 shows two such profiles collected with the HTB. Using multiple projections about the bone axis allows structural properties (e.g., bending strength) to be obtained independent of patient position. To do this, at least three arbitrary projections must

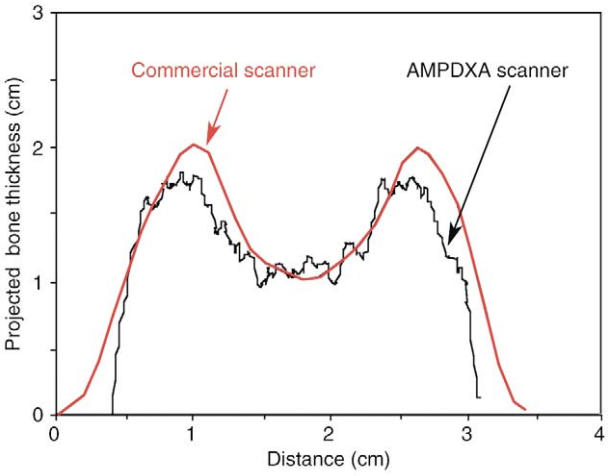

Figure 6. Bone mass profiles with distance across a given bone section for both the AMPDXA and a commercial scanner.

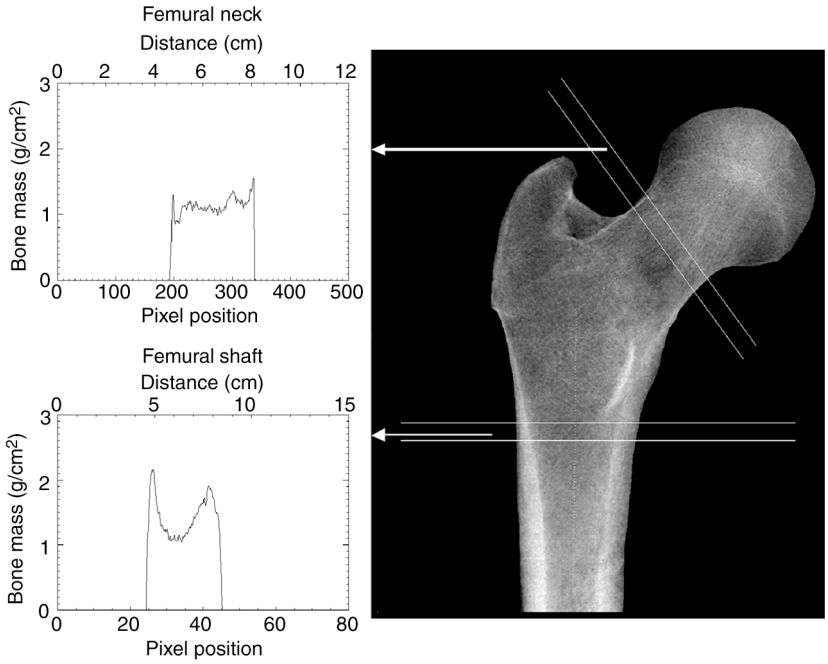

Figure 7. AMPDXA BMD image of a femur with two sectional slices indicated. The curves on the left represent bone mass profiles with distance across the given section.

be obtained. Projections can be over an angle as small as 30° (e.g., 0° and ±15°). With the LTB and HTB, the projections were typically made over a 90° angle. Such analyses can provide maximum and minimum moments of inertia for bending or torsion in any plane. We have shown that the error in the three-projection estimation of moments of inertia is approximately 1 to 2%. Additional projections (above three) may reduce this number further.

While impressive results have been achieved with the HTB, including high-resolution BMD images of a human hip (Fig. 8), the HTB has some limitations that must be overcome in the final AMPDXA space unit. The HTB lacks the flexibility to orient the X-ray beam along the prescribed cut planes. In addition, a flat panel detector design was chosen for its high-resolution capability. The large image area of the flat panel also makes scatter and glare an issue in pixel linearity. Thus, a special antiscatter grid (Fig. 9) and an algorithm for removing optical glare were developed. Because of its deep, evenly spaced slots, the grid removes most of the scatter (off-axis X-rays) but leaves some vertical striping artifacts (Fig. 10). Another by-product of the grid is that the time to complete a three-projection imaging sequence is longer than desirable. Additional work on a more sophisticated glare correction technique based on a deconvolution of the glare point-spread function is being conducted. Because the antiglare grid obscures 50% of the X-rays impinging on the detector caused by the size of the grid plates, two images at each energy (and angular position) must be taken—one with the grid in the home position and another in a shifted position (shift distance equals the thickness of a grid plate) so that a full area image can be obtained. The AMPDXA GCS described later in this article will overcome these limitations.

Data Processing

The multiple-projection capability and the high-resolution images produced by the AMPDXA are the key elements for processing the data and determining bone parameters. A multistep data acquisition process obtains data at dual energies generated by two different voltages applied to the X-ray tube—80 kilovolts peak (kV_p) and 140 kV_p—at three different projections offset by known angles. Currently, we are using a 15° offset. The 15° interval for the different projections was selected because it was large enough to extract geometrical data for the principal moments of inertia, yet small enough to prevent other anatomical parts from obstructing the

Figure 8. BMD image of the human hip of a live subject based on an aluminum thickness decomposition with the improved antiscatter grid.

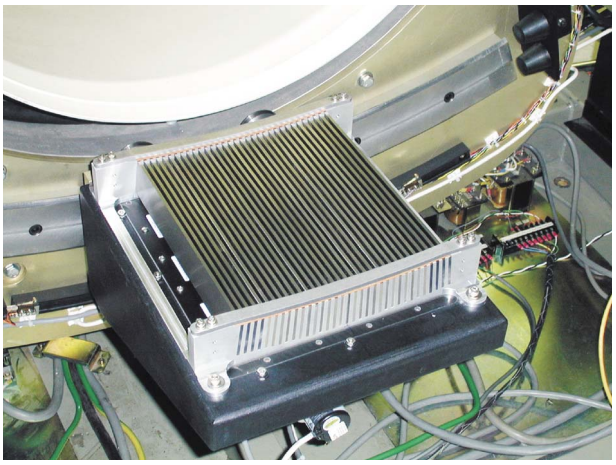

Figure 9. Photograph of the high-performance antiscatter grid mounted over the flat panel detector of the HTB.

imaging of the bone of interest. After acquisition, the data are processed by software developed by the AMPDXA team. The present HTB processing and analysis software is written in Interactive Data Language (IDL).

The software then identifies and processes 12 image files acquired during the testing of one patient. The 12 files are from the three projections (0°, ±15°), the two offsets (of the antiscatter grid) at each angle, and the two different kilovolt exposures at each angular position. The software also identifies and reads AMPDXA hardware settings for each file, including dosimeter recordings for each exposure. In addition, it uses two reference images from exposures with nothing in the beam and numerical results derived from calibration data. The main outputs of the current AMPDXA software are bone structural properties and high-resolution BMD images. Examples of images produced by the HTB for various steps of the process are illustrated in Fig. 10.

The following is a summary of the eight fundamental processing steps[19]:

1. *Read raw image files and format images*. The detector has some unused pixels at the edges that are cropped, and the total image size is rescaled by a factor of 2 for computational efficiency.
2. *Isolate antiscatter grid position and remove glare in each image*. A template or mask is created where the antiscatter grid is located. Pixel values under the grid are curve-fit across the image to estimate the optical glare effects, which are then subtracted out.
3. *Combine home position and shifted position images*. "Sew" together two image halves to form a "full" image. Because of dose variations between the home and shifted images, the images are scaled appropriately based on the measured dose before they are combined.
4. *Compute attenuation for each pixel at low and high energies*. The equations below show how the low- and high-energy attenuations are calculated using the image pixel value V_{low} or V_{high} relative to the blank image (nothing in the beam) recorded prior to image acquisition, $V_{0_{low}}$ or $V_{0_{high}}$. They are also scaled (S_{low} or S_{high}) based on actual doses during exposure:

$$L_{attn} = -\log_{10}\frac{V_{low}}{V_{0_{low}} \times S_{low}},$$

and

$$H_{attn} = -\log_{10}\frac{V_{high}}{V_{0_{high}} \times S_{high}}.$$

5. *Compute decomposition images of equivalent aluminum and plastic images*. This algorithm is based on techniques described by several authors.[20,21] Using a phantom constructed at APL with 77 different thicknesses of plastic (to simulate soft tissue) and aluminum (to simulate bone), data are acquired and fit to

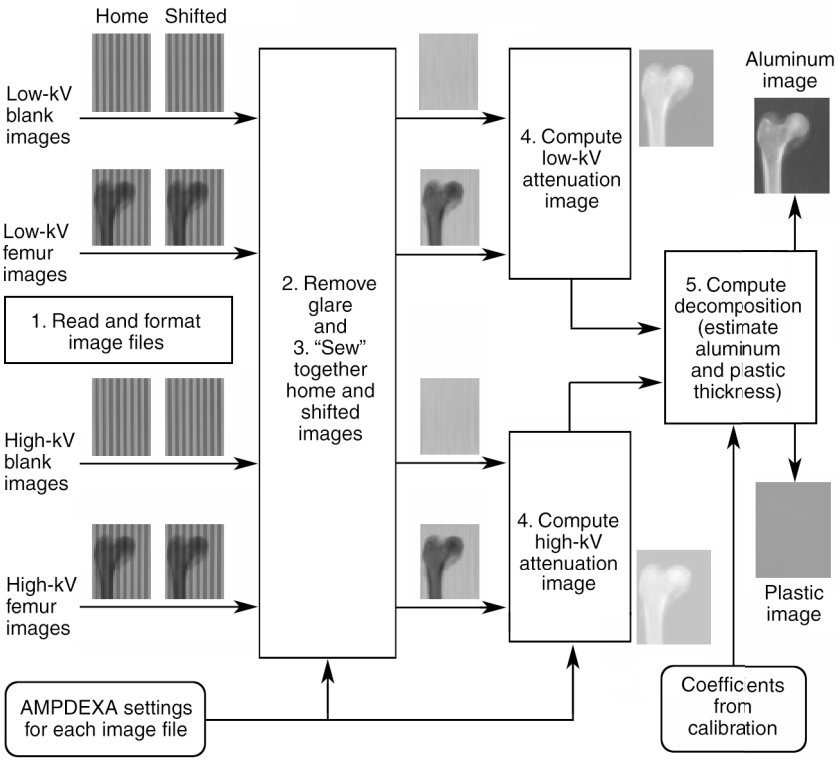

Figure 10. Images produced by the HTB as it goes through the first five steps in the basic processing sequence.

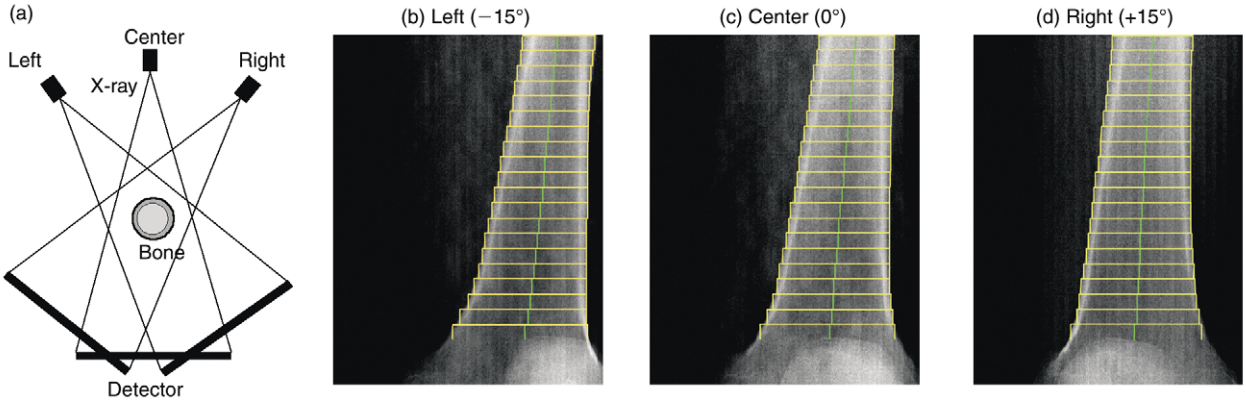

Figure 11. AMPDXA multiple projections using the restricted angle concept (0°, ±15°). (a) Diagram of three projections showing cone beam geometry and rotational capability. (b)–(d) Processed AMPDXA BMD images of the human femur for the three projections.

calibration curves. Using the equations below, plastic and aluminum images are obtained from the calibration coefficients (identified as q_n) and the low- and high-energy attenuation images:

$$\text{plastic} = q_1 L_{\text{attn}} + q_2 H_{\text{attn}} + q_3 L_{\text{attn}}^2 + q_4 H_{\text{attn}}^2 + q_5 L_{\text{attn}} H_{\text{attn}} ,$$

and

$$\text{aluminum} = q_6 L_{\text{attn}} + q_7 H_{\text{attn}} + q_8 L_{\text{attn}}^2 + q_9 H_{\text{attn}}^2 + q_{10} L_{\text{attn}} H_{\text{attn}} .$$

6. *Compute tissue equivalent values*. Image processing techniques such as thresholding and segmentation are used to isolate only the pixels representing bone regions in the X-ray images. For these pixels, the equivalent aluminum and plastic images are used in the mathematical formulations below for bone tissue mass. In the bone mass image, each pixel, in units of g/cm^2, is then divided by bone density of 1.05 g/cm^2, which results in an equivalent linear thickness in centimeters:

$$\text{bone mass} = \text{aluminum} \times 1.052074015 + \text{plastic} \times 0.014602233 .$$

7. *Compute bone cross sections and bone structural properties*. These parameters (diameter, area, moments of inertia, etc.) are calculated over cross sections approximately 5 mm thick along the bone axis, as shown in Fig. 11 and Tables 1 and 2.
8. *Calculate center-of-mass axis of bone in 3D coordinates*. Data from each projection are combined to determine the bone position in 3D coordinates relative to the X-ray source and detector.

Analysis

Center of Mass

Figure 11 shows three bone mass images of the human femur of a live subject (the patella is shown in the lower part of each image) at each of three projections. The long axis of the bone is sectioned into 5-mm-thick slices as indicated by the yellow horizontal lines in Figs. 11b–d.

Table 1. AMPDXA structural measurement results on artificial bone cylinders compared to actual cylinder data.

Parameter	AMPDXA	Actual	Difference (%)
Diameter (cm)	2.17	2.20	−1.36
Cross-sectional area (cm^2)[a]	2.28	2.26	+0.88
Moment of inertia, I_x (cm^4)	0.96[b]	0.96	−0.53
Moment of inertia, I_y (cm^4)	0.93	0.96	−3.13

[a]Since the cylinders were hollow, the given cross-sectional area is for the annular ring of material in the beam.
[b]0.955 to the next decimal place.

Table 2: Standard deviations for repeated measurements of key structural parameters on a cadaver femoral shaft.

Parameter	Standard deviation
Diameter (cm)	±0.019
Cross-sectional area (cm^2)[a]	±0.012
Moment of inertia, I_x (cm^4)	±0.021
Moment of inertia, I_y (cm^4)	±0.033

[a]Since the cylinders were hollow, the given standard deviation is for the cross-sectional area of the annular ring.

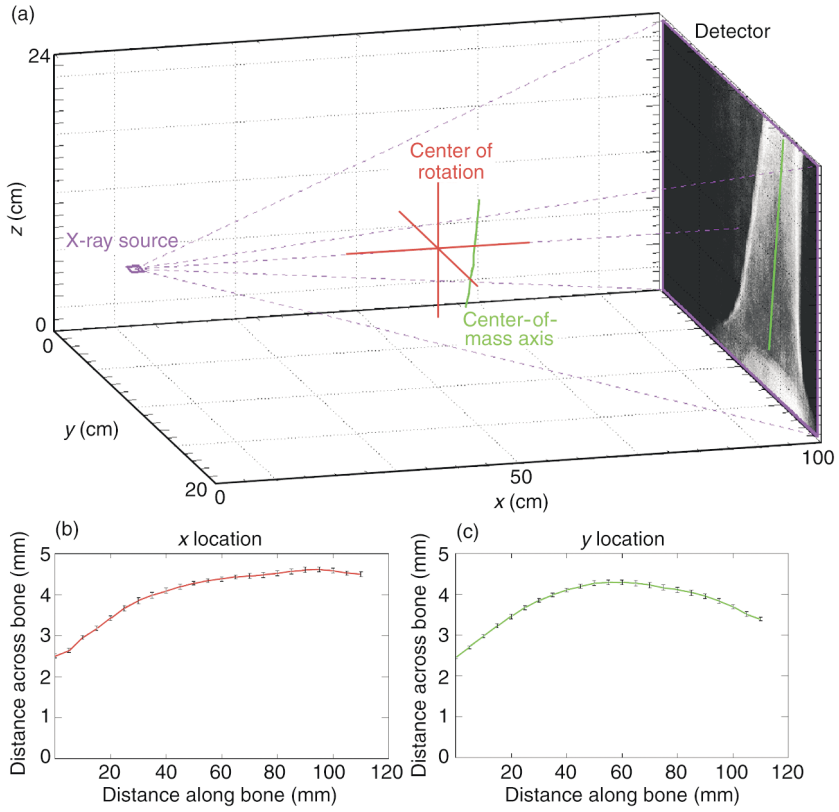

Figure 12. (a) Center-of-mass axis of the human femur in 3D relative to the source and the detector. The *x* and *y* locations, (b) and (c), respectively, of the center of mass along the bone for five repeated measurements and calculations.

Within each slice, the location of the center of mass is marked by the green line. Figure 12 illustrates the center-of-mass axis plotted in a 3D coordinate system for the data of Fig. 11. Because the time position is known within the 3D system of coordinates along with the projected beam geometry, accurate geometrical and structural calculations can be made.

Accuracy

To assess the accuracy of the AMPDXA system, several cylinders of different thicknesses were constructed from an artificial bone simulant. These cylinders were then scanned by the AMPDXA, and the resultant structural parameters were calculated and compared to actual values derived from mechanical measurements of the test specimens. The test cylinders were also placed at several different locations within the cone beam geometry to verify consistent results.

Table 1 summarized results from a typical cylinder that indicate repeatable accuracies for all structural parameters in the 1 to 3% range, with some much less than 1%. The standard deviations of all measurements (Table 2) were in fractions of millimeters, which is roughly the size of a pixel.

To test precision, we repeated data collection five times on a human cadaver femur submersed in a canister of water (simulates soft tissue). The structural parameters (center-of-mass diameter, cross-sectional area, and moments of inertia) were calculated for 23 slices (each 5 mm thick) at 5-mm intervals for all five data collections. The calculated parameters from all five were very similar. For example, the largest standard deviation of the center-of-mass axis location along the *x* axis (along the direction of the X-rays) was 0.15 mm. This is slightly larger than the detector pixel size. In the *y* dimension, the standard deviation was 0.07 mm, which is less than the pixel size. The diameter, cross-sectional area, and moments of inertia also showed consistent results.

Applications

The AMPDXA project has many implications for future research and development. As noted earlier, it has direct application to risk reduction in NASA's Critical Research Path. The AMPDXA is capable of real-time monitoring of bone and muscle loss, at any anatomical location, with extremely high precision. Since the results are patient-specific and not tied to volumetric averages and statistical norms, the AMPDXA is a useful tool for monitoring the effectiveness of countermeasures as well as determining the risk of fracture under various loading conditions and activity scenarios. It also appears to be a natural adjunct to earthbound research on the effect of aging and disuse on bone integrity and could be used as a routine screening tool for osteoporosis and as a monitoring instrument for osteoporosis drug therapy.

Since the AMPDXA measures structure to high precision and does an excellent job at imaging not only bone but also man-made prosthetic implants, it could be used by orthopedic surgeons to study the life progression of implants (e.g., loosening, bone regression, etc.). Given its low radiation dose and ability to automatically determine dimensions from the collected radiographic data, the AMPDXA may prove valuable in other orthopedic applications as well. For example, it is possible to predict stress fractures from BMD measurements.[22] Stress fractures in military recruits range from 1 to 7%, depending on gender and branch of service. An untold number of athletes and others also suffer stress fractures annually as a result of intense, repetitive exercise.[23] Such exercise or other similar activity can tire muscles

so that they can no longer absorb the shock from these activities. This causes tiny hairline cracks known as stress fractures to develop in the bone. The best treatment for stress fractures is rest for 6 to 8 weeks. Such rest periods would prevent a professional athlete or a soldier from performing his/her job. Thus, the ability to identify people susceptible to stress fractures would enable a different training regimen to prevent the onset of these fractures.

As noted earlier, to facilitate the space application, APL is developing the AMPDXA GCS instrument for the ground-based testing of astronauts (pre- and post-flight) at Johnson Space Center, Houston, Texas. The GCS detection scheme, which is based on a novel design not found in conventional DXA imaging systems, will use small arrays of single-element detectors. This design mitigates cone beam issues and nonlinearities caused by scatter and optical glare. Furthermore, it lowers costs when compared to the flat-panel detector used in the LTB and the HTB.

As illustrated in Fig. 13, the AMPDXA GCS scanner uses three detector modules at the top of a C-arm that are mechanically aligned to the X-ray tube at the bottom of the C-arm. One detector module is located along a line perpendicular to the table plane; the other two are displaced 15° to either side of the center module relative to the tube focus. Each module contains thirty-two 1.5×1.5 mm elements in two staggered rows of 16 elements each. The staggered rows permit oversampling in each image dimension at the Nyquist rate. Unlike other designs, the sampling and spatial resolution will be equal in each image dimension. Because of the arrangement of the detector modules, projections at 0° and ±15° are obtained with a single horizontal transit of the C-arm across the patient.

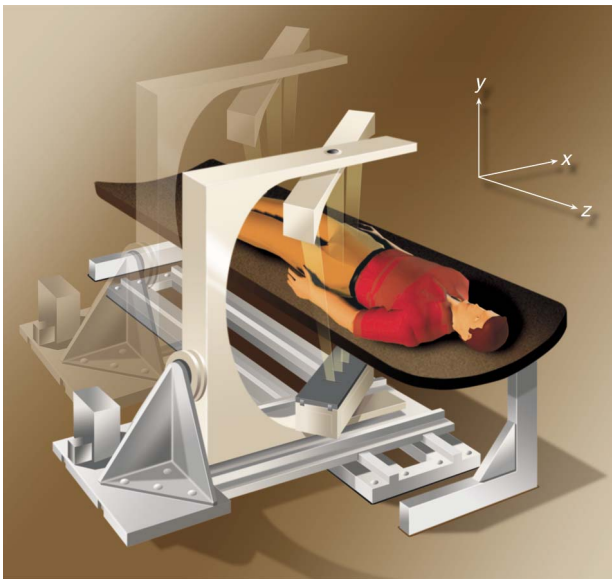

Figure 13. Artist's concept of the AMPDXA Ground-based Clinical System.

THE FUTURE

The AMPDXA is moving forward on several fronts. The HTB will be used to determine the *in vivo* precision and accuracy of the AMPDXA. The standard of comparison will be DXA scans using a modern, commercial, conventional DXA scanner. Also, *in vivo* muscle and fat measurements will be performed and compared to results from the conventional DXA scanner. Similar work on software algorithms for the extraction of soft tissues, bone reconstruction, and the relationship of bone strength to the risk of fracture will be conducted. Software (and instrumentation) refinements will also be necessary to permit the collection of radiographs for the diagnosis of injury and disease.

Commercially, if cost projections can be realized, there is a significant market for population screening and treatment monitoring of osteoporosis. Based on the AMPDXA GCS, an easy-to-use, relatively compact instrument could be developed for a small clinic or physician practice. The unit could be either horizontal like the GCS or vertical (patient stands). Concepts for a vertical unit have been developed. The market for such a commercial AMPDXA could range from several hundred to several thousands of units, depending on final cost. If the unit could be structured to be lightweight and relatively transportable, it would have important implications for use as a tool in nursing homes, clinics, and physicians' offices. Several key members of the NSBRI's Bone Research Team have already indicated that a precision AMPDXA would greatly assist their work in bone loss investigations, especially in bed rest studies.

AMPDXA commercialization efforts are being pursued by both the APL Technology Transfer Office and the Technology Transfer Office of the Johns Hopkins Medical Institutions. Commercialization of the AMPDXA software for use with conventional DXA data may provide the stepping-stone for the commercialization of the AMPDXA hardware.

REFERENCES

[1]Oganov, V. S., Grigurèv, A. I., Voronin, L. I., Rakhmanov, A. S., Bakulin, A. V., et al., "Bone Mineral Density in Cosmonauts After Flights Lasting 4.5–6 Months on the Mir Orbital Station," [in Russian] *Avia Kosim-Ekolog Med.* **26**, 20–24 (1992).

[2]LeBlanc, A. D., Rowe, R., Schneider, V., Evans, H., and Hedrick, T., "Regional Muscle Loss After Short Duration Space Flight," *Aviat. Space Environ. Med.* **66**(12), 1151–1154 (Dec 1995).

[3]Vogel, J. M., and Whittle, M. W., "Bone Mineral Content Changes in the Skylab Astronauts," in *Proc. Am. Soc. Roentgenol.* **126**, pp. 1296–1297 (1976).

[4]Wahner, H., "Use of Densitometry on the Measurement of Osteoporosis," in *Osteoporosis*, R. Marcus, D. Feldman, and J. Kelsey (eds.), Academic Press, pp. 1055–1074 (1996).

[5]Kiralti, B., "Immobilization Osteopenia," *Osteoporosis*, R. Marcus, D. Feldman, and J. Kelsey (eds.), Academic Press, pp. 833–853 (1996).

[6]"The State of the Art in the Management of Osteoporosis," *Interdiscipl. Med.* **5**(5) (Jan 2004).

[7]Beck, T. J., Ruff, C. B., Scott, W. W. Jr., Plato, C. C., Robin, J. R., and Quan, C. A., "Sex Differences in Geometry of the Femoral Neck with Aging: A Structural Analysis of Bone Mineral Data," *Calsified Tissue Int.* **50**, 24–29 (1992).

[8]Whitson, P. A., Pietrzyk, R. A., Pak, C. Y. C., and Cintrón, N. M., Alternations in Renal Stone Risk Factors After Space Flight," *J. Urol.* **150**(3), 803–807 (1993).
[9]Bioastronautics Critical Path Roadmap, Baseline Document, *An Approach to Risk Reduction and Management for Human Space Flight*, Rev. D, Critical Path Control Panel, Bioastronautics Program Office, NASA Johnson Space Center, http://criticalpath.jsc.nasa.gov/ (30 Jul 2003).
[10]Nicogossian, A. E., Sawin, C. F., and Grigoriev, A. I., "Countermeasures to Space Deconditioning," in *Space Physiology and Medicine*, 3rd Ed., A. E. Nicogossian, C. L. Huntoon, and S. L. Pool (eds.), Lea and Febiger Publishers, Philadelphia, PA, pp. 447–467 (1994).
[11]Davis, B. L., D'Andrea, S. E., Hoadley, D., and Truang, T., "Design of a High Force Exercise Device," in *Abstract Book, Bioastronautics Investigators' Workshop*, Galveston, TX, p. 84 (13–15 Jan 2003).
[12]National Space Biomedical Research Institute (NSBRI) Web site, www.nsbri.org.
[13]Pouelles, J. M., Trewollieres, F., and Ribot, C., "Spine and Femur Densitometry at the Menopause: Are Both Sites Necessary in the Assessment of Risk of Osteoporosis?" *Calsified Tissue Int.* **52**, 344–347 (1993).
[14]Nyenhuis, J. A., Bourland, J. D., Kildishev, A. V., and Schaefer, D. J., "Health Effects and Safety of Intense Gradient Fields," Chap. 2, in *Magnetic Resonance Procedures: Health Effects and Safety*, F. G. Shellook (ed.), ORC Press, pp. 31–54 (2000).
[15]Faulkner, K. G., von Stetten, E., and Miller, P., "Discordance in Patient Classification Using T-Scores," *J. Clin. Densitom.* **2**(3), 343–350 (1999).
[16]Deng, H-W, Li, J-L., Li, J., and Davies, K. M., "Heterogeneity of Bone Mineral Density Across Skeletal Sites and Its Clinical Implications," *J. Clin. Densitom.* **1**(4), 339–353 (1998).
[17]Qin, Y-X., Mittra, E., Lin, W., Xia, Y., and Rubin, C., "Non-invasive Assessment of Bone Strength and Density Using Scanning Ultrasound," in *Proc. ASME-BED Bioengineering Conf.* **51**, pp. 373–374 (2003).
[18]Charles, H. K. Jr., Beck, T. J., Feldmesser, H. S., Magee, T. C., Spisz, T. S., and Pisacane, V. L., "Precision Bone and Muscle Loss Measurements by Advanced Multiple Projection DEXA (AMPDXA) Techniques for Space Flight Applications," *Acta Astronaut.* **49**(3–10), 447–450 (2001).
[19]Spisz, T. S., Beck, T. J., Feldmesser, H. S., Chen, M. H., Magee, T. C., et al., "Determination of Bone Structural Parameters from Multiple Projection DXA Images," in *Medical Imaging 2004*, San Diego, CA, pp. 730–741 (15–17 Feb 2004).
[20]Cardinal, H. N., and Fenster, A., "An Accurate Method for Direct, Dual Energy Calibration and Decomposition," *Med. Phys.* **17**(1), 327–341 (1990).
[21]Lehmann, L. A., Alvarez, R. E., Macovski, A., Brody, W. R., Pelc, N. J., et al., "Generalized Image Combinations in Dual V_p Digital Radiography," *Med. Phys.* **8**(5), 659–667 (Sep/Oct 1981).
[22]Beck, T. J., Ruff, C. B., Mourtada, F. A., Shaffer, R. A., Maxwell-Williams, K., et al., "Dual Energy X-ray Absorptiometry Derived Structural Geometry for Stress Fracture Prediction in Male U.S. Marine Corps Recruits," *J. Bone Miner. Res.* **11**, 645–653 (1996).
[23]Beck, T. J., Ruff, C. B., Shaffer, R. A., Betsinger, K., Trone, D. W., and Barodine, S. K., "Stress Fracture in Military Recruits: Sex Differences in Muscle and Bone Susceptibility Factors," *Bone* **27**(3), 437–444 (2000).

ACKNOWLEDGMENTS: The authors gratefully acknowledge the efforts of the following people, without whose support the AMPDXA accomplishments described in this article could not have been achieved: Paul Bade and Michael Reid for JAVA software development, Sterling Smoot for data collection hardware and software contributions, Wolfger Schneider and Jennifer Nix for improvements in hardware operation, Wil Chung for driver software development, Robert Geller and Shirley Drabek for mechanical fabrication and electrical wiring, and Michelle Rockwell for software development for the LTB. A special thank you is extended to Frona A. Steelman and S. Lynn Hoff for their help in manuscript preparation. The NSBRI is funded under Cooperative Agreement NCC-9-58 with the NASA Lyndon B. Johnson Space Center, Houston, TX.

THE AUTHORS

The AMPDXA-GCS Team is led by **Harry K. Charles Jr.**, the AMPDXA-GCS project Principal Investigator (PI). Dr. Charles is an APL Principal Professional Staff member and heads the Laboratory's Technical Services Department. For the AMPDXA-GCS, he provides overall project management and contributes to the design and packaging of the instrument. **Michelle H. Chen** is a systems engineer in APL's National Security Technology Department. For the AMPDXA-GCS, she is responsible for providing the instrument movement and control software, as well as assisting in project management. **Thomas S. Spisz** is an electrical engineer in APL's Space Department and is responsible for the development of the image analysis software for the AMPDXA-GCS. **Thomas J. Beck** is an Associate Professor of radiology at the Johns Hopkins University School of Medicine. He is the Co-PI for the AMPDXA-GCS project, providing technical input on X-ray imaging and bone structural measurement. **Howard S. Feldmesser** is a Principal Professional Staff electrical engineer in the Technical Services Department and a Certified Clinical Engineer. He provides electrical design, fabrication, and assembly, as well as oversight of machine safety and operation. **Thomas C. Magee** is a mechanical engineer in APL's Technical Services Department and is responsible for all mechanical design, fabrication, and assembly. **Barry P. Huang** (not pictured) is a first-year biomedical student at the University of Pennsylvania and worked with the AMPDXA-GCS Team as a summer student, studying bone loss mechanisms and countermeasures. The AMPDXA-GCS Team can be contacted through the PI, Dr. Charles. His e-mail address is harry.charles@jhuapl.edu.

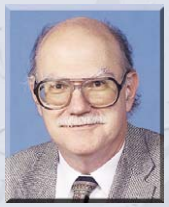
Harry K. Charles Jr.


Michelle H. Chen


Thomas S. Spisz


Thomas J. Beck


Howard S. Feldmesser


Thomas C. Magee